Atmos. Chem. Phys. Discuss., 15, 31925–31950, 2015
www.atmos-chem-phys-discuss.net/15/31925/2015/
doi:10.5194/acpd-15-31925-2015

Atmospheric Chemistry and Physics Discussions

Tropospheric Ozone Variability during the East Asian Summer Monsoon as Observed by Satellite (IASI), Aircraft (MOZAIC) and Ground Stations

S. Safieddine[1,a], A. Boynard[1], N. Hao[2], F. Huang[3], L. Wang[4], D. Ji[4], B. Barret[5], S. D. Ghude[6], P.-F. Coheur[7], D. Hurtmans[7], and C. Clerbaux[1,7]

[1]Sorbonne Universités, UPMC Univ. Paris 06, Université Versailles St-Quentin, CNRS/INSU, LATMOS-IPSL, Paris, France
[2]German Aerospace Center (DLR), Remote Sensing Technology Institute (IMF), Oberpfaffenhofen, Germany
[3]National Satellite Meteorological Center, China Meteorological Administration, Beijing, China
[4]Institute of Atmospheric Physics, Chinese Academy of Sciences, Beijing, China
[5]Laboratoire d'Aérologie, Observatoire Midi-Pyrénées, Université Paul Sabatier, CNRS, Toulouse, France
[6]Indian Institute of Tropical Meteorology, Pashan Rd., Pune-411 008, India
[7]Spectroscopie de l'Atmosphère, Chimie Quantique et Photophysique, Université Libre de Bruxelles (U.L.B.), Brussels, Belgium

[a]now at: Department of Civil and Environmental Engineering, Massachusetts Institute of Technology, Cambridge, MA, USA

Received: 19 August 2015 – Accepted: 5 November 2015 – Published: 13 November 2015

Correspondence to: S. Safieddine (sarahsaf@mit.edu)

Published by Copernicus Publications on behalf of the European Geosciences Union.

ACPD
15, 31925–31950, 2015

Abstract

Satellite measurements from the thermal Infrared Atmospheric Sounding Interferometer (IASI), the Measurements of OZone and water vapor by in-service AIrbus airCraft (MOZAIC), as well as observations from ground based stations, are used to assess the tropospheric ozone (O_3) variability during the East Asian Summer Monsoon (EASM). Six years [2008–2013] of IASI data analysis reveals the ability of the instrument to detect the onset and the progression of the monsoon reflected by a decrease in the tropospheric [0–6] km O_3 column due to the EASM, and to reproduce this decrease from one year to the other. Focusing on the period of May–August 2011, taken as an example year, IASI data show clear inverse relationship between tropospheric [0–6] km O_3 on one hand and meteorological parameters such as cloud cover, relative humidity and wind speed, on the other hand. Aircraft data from the MOZAIC project at Hyderabad, Nanjing and Guangzhou are used to validate the IASI data and to assess the effect of the monsoon on the vertical distribution of the tropospheric O_3 at different locations. Results show good agreement with a correlation coefficient of 0.74 between the [0–6] km O_3 column derived from IASI and MOZAIC. The aircraft data show a decrease in the tropospheric O_3 that is more important in the free troposphere than in the boundary layer and at Hyderabad than at the other two Chinese cities. Ground station data at different locations in India and China show a spatiotemporal dependence on meteorology during the monsoon, with decrease up to 22 ppbv in Hyderabad, and up to 5 ppbv in the North China Plain.

1 Introduction

Over South and East Asia, tropospheric ozone (O_3) concentrations have significantly increased over the past few decades as a result of rapid urbanization (Cooper et al., 2014) with important implications on regional and global air quality. South and East Asian countries are experiencing increasing emissions of different pollutants, many of

ACPD
15, 31925–31950, 2015

which are precursors of O_3 (Akimoto, 2003; Ohara et al., 2007; Richter et al., 2005). For example, China showed an increase of NO_2 reaching 29 % per year for the period 1996–2006 (van der A et al., 2008), and about 50 % over the industrial areas of China over the period 1996–2004 (Richter et al., 2005), though recent NO_2 observations from space are suggesting NO_2 decrease in 2013 and 2014 (Richter et al., 2015). An increase in background O_3 concentrations is also detected in Southern China during the last decade (Wang et al., 2009). In Eastern China, a study by Xu et al. (2008), analyzing long term trends at a background surface O_3 station in Linan, suggests enhanced O_3 variability linked to the increase in NO_x ($NO_x = NO_2 + NO$) concentrations. Over most India, increasing trends in tropospheric O_3 are consistent with the observed trends in emissions from NO_x and carbon monoxide (CO) as well as coal and petroleum consumption (Lal et al., 2012).

The Asian monsoon circulation dominates the regional meteorology of southern and East Asia. In summer, the East Asian Summer Monsoon (EASM) is characterized by torrential rain, strong winds carrying clean air from the ocean over the heated tropical land and deep convection processes forming cirrus clouds and further rain (Lawrence and Lelieveld, 2010). Surface observations have shown that the EASM is responsible for a decrease in surface O_3 at a rural site near Beijing (Wang et al., 2008) and a coastal site near Hong Kong (Lam et al., 2001; Wang et al., 2009). Yang et al. (2014) found that the largest impacts of EASM on the decrease in surface O_3 are found over central and western China, while Beijing (North East China) and Nanjing (East China) experience a summertime O_3 maxima during June and July respectively (Ding et al., 2008, 2013). Ozonesondes measurements have also detected the effect of the EASM on lower tropospheric O_3 (Chan et al., 1998; Zhou et al., 2013). Satellite measurements over South and East Asia have been used to assess the daily variability of tropospheric O_3, notably from the Infrared Atmospheric Sounding Interferometer (IASI) (Dufour et al., 2015). The effect of the EASM on the tropospheric O_3 was previously detected with a decrease in the O_3 partial column using data from IASI over several Indian and Chinese cities (Dufour et al., 2010; Safieddine et al., 2013). Using the Ozone Monitoring

ACPD
15, 31925–31950, 2015

Instrument (OMI) and Microwave Limb Sounder (MLS) measurements, together with a regional chemistry and transport model, Zhao et al. (2010) showed that the air quality over southeastern China is affected by the EASM, leading to an influence extending to central East China from June to July. At 300 hPa, the Tropospheric Emission Spectrometer (TES) observations over India showed enhanced O_3 abundances during June and July followed by a decrease in August (Worden et al., 2009).

The main objective of this study is to document the effect of the monsoon on the regional and vertical distribution of tropospheric O_3 in East Asia during the summer using different observation datasets and relating them to one another. After this introduction, Sect. 2 will look at six years of tropospheric [0–6] km O_3 data. Section 3 will focus on the monsoon of 2011, documented by a dense set of vertical O_3 airborne profiles and five ground stations dataset. We study the relationship between the tropospheric [0–6] km O_3 column from IASI and different meteorological parameters from the ECMWF (European Centre for Medium-Range Weather Forecasts) Reanalysis (ERA) (winds, cloud cover and relative humidity) (Dee et al., 2011). We then use aircraft profiles, to first validate the IASI observations and second to look at the effect of the monsoon on the vertical profiles of O_3 at three different locations (Hyderabad, Guangzhou and Nanjing). We finally examine ground stations at five locations (Hyderabad, Udaipur, Jabalpur, Pearl River Delta (PRD) and North China Plain (NCP)) during the EASM of 2011. Conclusions are given in Sect. 4.

2 Tropospheric O_3 from IASI

2.1 The IASI instrument

The IASI instruments launched onboard the MetOp platforms in October 2006 (IASI-A) and September 2012 (IASI-B) are nadir looking Fourier transform spectrometers that probe the Earth's atmosphere in the thermal infrared spectral range between 645 and 2760 cm^{-1}, with a spectral resolution of 0.5 cm^{-1} (apodized) and 0.25 cm^{-1} spectral

ACPD
15, 31925–31950, 2015

sampling. In this study, and to have a consistent O_3 product over the period 2008–2013, only IASI-A data have been used. The IASI footprint is a matrix of 2×2 pixels, each with 12 km diameter at nadir. IASI monitors the atmospheric composition at any location two times per day (the satellite's ground track is at about 9:30 a.m. and 9:30 p.m. local time). Each IASI measures many of the chemical components that play a key role in the climate system and in several aspects of atmospheric pollution. Global distributions of O_3 vertical profiles are retrieved in near real time using a dedicated radiative transfer and retrieval software for the IASI O_3 product, the Fast Optimal Retrievals on Layers for IASI (FORLI-O_3) (Hurtmans et al., 2012). Data are selected using a filter for scenes with no or low cloud coverage (below 13 %), and by rejecting all observations with root mean square (RMS) of the spectral fit residual larger than 3.5×10^{-8} W cm^{-2} sr cm^{-1}. Details about the chemical components that can be measured by IASI can be found in Clerbaux et al. (2009), Coheur et al. (2009) and Clarisse et al. (2011).

2.2 Tropospheric O_3 during the EASM for 2008–2013

To look at the inter-seasonal and inter-annual variation of tropospheric O_3 during the monsoon, we show in Fig. 1 the monthly distribution (May–September) of the IASI [0–6] km O_3 column over the period 2008–2013. Only IASI daytime observations are used, since better thermal contrast, and hence better sensitivity to the lower troposphere, is usually obtained during the day (Clerbaux et al., 2009). Earlier studies have shown that the information content in the satellite measurement varies, and is generally maximal in the mid to upper troposphere, and lower at the surface (Barret et al., 2011; Dufour et al., 2012; Safieddine et al., 2014). The [0–6] km O_3 column is used to eliminate any possible stratospheric intrusions and previous studies have shown that with the [0–6] km column, at least one piece of information is available for the IASI retrieval (Barret et al., 2011; Dufour et al., 2012). Limitations in the sensitivity provide sources of error that can influence our conclusions about the observed O_3 distribution, especially close to the surface. Another source of error emerge from the fact that the IASI observations used here are for scenes (pixels) with no or low cloud contamination, and therefore

ACPD
15, 31925–31950, 2015

reflect mostly the state of the atmosphere before or after the rain/high cloud episodes that the EASM will generate. The monthly average tropospheric O_3 columns from IASI shown here have different observation count at each grid point, which may correspond to the average of one to more than 200 observations. Despite these limitations, this is the best-known dataset of remote infrared retrieved O_3 columns covering the entire monsoon region, and we assume that the average effect of the monsoon on the tropospheric O_3 column from one month to the other can be reflected in one or more observations.

The seasonal variation of O_3 as detected by IASI is highly dependent on photochemical activity and is generally higher in summer and lower in winter (Safieddine et al., 2013). However, within the EASM region, IASI shows in Fig. 1 that this typical seasonality is broken and on average, the [0–6] km O_3 columns are lower in June–July–August (JJA) in comparison with May. The Asian monsoon onset date is around the mid-May and June (Parthasarathy et al., 1994; Wang et al., 2009; Yang and Lau, 1998). Figure 1 shows that the largest decrease is recorded in Southern India, where clean air masses from the Pacific starting typically in May (generating the Indian Summer Monsoon, a subsystem of the EASM) will be responsible of a decrease reaching 15–20 Dobson Unit (DU) in JJA. With the march of the monsoon northeastward, the decrease becomes most prominent in July and August at higher latitudes. Over the different years, the seasonal variation is well reproduced but the decrease in the tropospheric O_3 column will change in magnitude depending on the monsoon strength. For example, in June 2010, around 30° N and 120–130° E, the Western North Pacific region shows void area of IASI retrievals (with white pixels) due to large cloud cover. The Western North Pacific Monsoon Index (WNPI, Wang and Fan, 1999) is the highest in 2010 over this region in comparison with the rest of the years shown here. On the other hand, 2011, is rather a typical monsoon season year, and will be used as a case study hereafter.

ACPD
15, 31925–31950, 2015

3 Case study of 2011

3.1 Tropospheric O_3 from IASI coupled with meteorology

In order to look at the O_3 response to change in meteorology during the monsoon, we show in Fig. 2 the monsoon period of 2011 taken as an example year of a typical monsoon. We consider different meteorological parameters in order to highlight the relationship between change in meteorology and the [0–6] km O_3 column. These are, the total cloud cover that gives an insight on the photochemical activity in the troposphere; relative humidity, since increasing water vapor increases O_3 loss as the production rate of the reactions $H_2O + O(^1D) \rightarrow 2OH$ increases (where $O(^1D)$ is the product of the photo-dissociation of O_3 in the presence of ultraviolet light); and finally we add wind force and direction to assess monsoon strength and possible transport. All of the three parameters are extracted from the ECMWF re-analysis (Dee et al., 2011). The data assimilation produces 4 analyses per day at 00:00, 06:00, 12:00 and 18:00 UTC at 37 pressure levels from 1000 to 1 hPa. Monthly means of total cloud cover, relative humidity at 850 hPa and u and v components of horizontal wind directions at 850 hPa are extracted over a grid size of $0.75^\circ \times 0.75^\circ$.

During the EASM, the southwesterly monsoon flow brings warm, wet and clean air masses from the Indian Ocean to South, South-East and East Asia. The winds at 850 hPa in Fig. 2 show a typical monsoon flow where in May and June, it mostly impacts South and Southeast Asia while the coastal region of East Asia is impacted by southeasterlies from the Pacific. In June, in particular, the monsoon becomes stronger as the wind force and the cloud cover (and therefore lower photochemical activity) increase over the regions $< 20^\circ$ N and a decrease in tropospheric O_3 is recorded over India, Bay of Bengal and South East China. During July and August, the monsoon reaches its maximal strength. Due to high cloud cover and strong winds, the tropospheric O_3 columns show a large decrease. The wind effect on O_3 has been detected before using IASI measurements (though for post-monsoon period), where elevated tropospheric

ACPD
15, 31925–31950, 2015

O_3 values over central and southern India are shown to decrease significantly with the crossing of tropical storms (Barret et al., 2011). Moreover, the figure shows how during the monsoon, a persistent high content in water vapor in the atmosphere is detected. Johnson et al. (1999) found that this O_3-water vapor anti-correlation is most effective in the background troposphere. Here, with the high winds coming from the marine (background) troposphere, the decrease can be also associated to the low O_3 transport by the monsoon flow.

Looking at particular regions, tropospheric [0–6] km O_3 columns in Korea and Japan show a decrease in particular in July for O_3, which coincides with the high cloud cover and relative humidity. On the other hand, and over North West of India and part of Pakistan, the low cloud cover and weak winds lead to the buildup of the high summer O_3 over this region, and with little to no transport, the persistence of the [0–6] km O_3 values. Looking at the winds plots over the different months, one can notice how the monsoon is stronger at the lower latitudes of the domain. Therefore the areas of Beijing, Tianjin and the North China Plain (black square in Fig. 2) in general are less affected by the monsoon and they show much weaker O_3 decrease. In fact, the persistence of O_3 during the monsoon season in Beijing was previously documented using aircraft data from the MOZAIC program which suggested a summertime O_3 maximum attributed to strong photochemical production (Ding et al., 2008). The other interesting region in China that shows little or no change is the area between the Chongqing and Sichuan province (and designated with a black circle in Fig. 2). This region does not exhibit any monsoon characteristics with low cloud cover and weak winds. This region is also between two mountains, making the persistence of O_3 during summer favorable.

3.2 Tropospheric O_3 from MOZAIC

The Measurements of OZone and water vapor by in-service AIrbus airCraft (MOZAIC) program currently known as the European In-service Aircraft for a Global Observing System (IAGOS) program (Nedelec et al., 2015), has provided in situ observations of ozone, water vapor, carbon monoxide and other trace gases made from

ACPD
15, 31925–31950, 2015

multiple commercial aircraft since 1994 (Marenco et al., 1998; Thouret et al., 1998; http://www.iagos.org). In this study, we examine the monsoon effect on the vertical profile of tropospheric O_3 during the EASM of 2011 over three locations: Hyderabad (India), Nanjing (East China) and Guangzhou (South China) which geographical locations are indicated by a square sign in Fig. 3. First, we perform a validation analysis of the IASI data with 68 profiles from aircraft take-off and landing and then we look at the monthly averaged vertical profile of tropospheric O_3 over these three sites.

3.2.1 Validation of IASI

The IASI-retrieved tropospheric O_3 product is not a real concentration profile, but an estimation of the true profile considering the ability of the instrument to discriminate different atmospheric layers. Therefore one cannot directly compare satellite-retrieved profiles with high-resolution in situ observations such as the aircraft data. Instead, each high-resolution O_3 profile measured by the aircraft needs to be convolved by the low-resolution IASI averaging kernel matrix with the a priori profile, following Rodgers (2000) formulation:

$$x_{\text{smoothed}} = x_{\text{a,IASI}} + A_{\text{IASI}}(x_{\text{MOZAIC}} - x_{\text{a,IASI}}) \quad (1)$$

Where x_{smoothed} is the smoothed profile that uses low-resolution measurement characteristics. A_{IASI} is the low-resolution averaging kernel matrix. x_{MOZAIC} is the high-resolution profile given by the aircraft, and $x_{\text{a,IASI}}$ is the low-resolution IASI a priori profile constructed from the McPeters/Labow/Logan climatology of O_3 vertical distribution, which combines long-term satellite limb measurements and measurements from ozonesondes (see McPeters et al., 2007; Hurtmans et al., 2012). Before the smoothing, the validation profile has to cover the whole retrieval altitude range, which is from the ground up to 41 km. The aircraft data used here cover altitudes till around 8 km for Nanjing, and 12 km for Hyderabad and Guangzhou. The aircraft data profiles were therefore completed by the same a priori used for IASI so that the matrix calculation of Eq. (1) is valid. We have also used a IASI spatial coincidence criterion of ±0.75°

ACPD
15, 31925–31950, 2015

(∼ 80 km) around the position of the aircraft half way of its ascent or descent (to and from cruising altitude). In this section, both IASI day and nighttime observations are used for the validation of the aircraft data, so that the temporal coincidence is ±12 h.

Figure 4 shows the correlation of [0–6] km O_3 column retrieved from spatio-temporal coincidence of IASI and MOZAIC (smoothed profiles during May–August 2011) over Hyderabad ($N = 21$ profiles), Guangzhou ($N = 23$) and Nanjing ($N = 24$). The figure shows good correlation between the two datasets with $r = 0.74$ and an absolute bias of 2.7 ± 3.5 DU (16 % ± 22 %) suggesting a good ability of IASI to reproduce O_3 variability in the troposphere over this region. Discrepancies arise from the spatial resolution of the IASI footprint resulting in an observation averaged over several tens of kilometers around the airport and therefore may include other surface O_3 contributions. Moreover, the aircraft observation takes place at different times during the day whereas IASI observation is at around 9:30 a.m. and 9:30 p.m. local time. With its limited sampling time during the day and its lower sensitivity towards the surface, IASI observation won't be able to capture the diurnal variation of O_3 like an aircraft profile. However, since the satellite sensitivity increases with altitude, where the O_3 has a smaller diurnal variation, the comparison is possible. Averaged over the whole [0–6] km column, as in Fig. 4, our results are in good agreement with a validation done by Barret et al. (2011) based on 6 months of MOZAIC data to validate IASI data over India where they reported a correlation coefficient of 0.87 (12 % ± 6 %) between IASI tropospheric O_3 product (< 250 hPa) and MOZAIC aircraft data.

3.2.2 Monsoon effect on the vertical profiles

We show in Fig. 5 the monthly averaged (with the error bars as standard deviation) raw MOZAIC profiles during the EASM of 2011.

At Hyderabad (panel a), and from May to June, a clear decrease of around 30 ppbv in O_3 volume mixing ratios (VMR) is recorded at the surface. At higher altitudes up to around 6 km, an important decrease is also detected from May to June and then from June to both July and August. With a small standard deviation around the O_3 profiles,

ACPD
15, 31925–31950, 2015

the observation around Hyderabad suggests consistent averaged monthly behavior and shows a decrease in the O_3 profile at different altitudes from 0 to 6 km, which was also seen over the whole [0–6] km O_3 column from IASI in Figs. 1 and 2. At Guangzhou (panel b), the O_3 VMR in the lower troposphere decreases from May to June up to 20 ppbv at the surface but then increases back in July and/or August. At [5–8] km, the different months averaged O_3 VMR becomes comparable. Looking at the location of Guangzhou and at Fig. 2, we can see how the decrease in the lower tropospheric O_3 in June can be explained by the increase in the cloud cover and in particular an increase in the wind speed at 850 hPa coming from the west Pacific. Nanjing (panel c) is located in the Yangtze River Delta and will exhibit the monsoon effect starting the month of June (later than Guangzhou). Except at the surface, a decrease in the O_3 VMR is detected from June to July and August (till 6 km).

3.3 Ground-based measurements

The MOZAIC profiles illustrated in Fig. 5 have shown that the effect of the EASM on surface/boundary layer O_3 largely depends on the location. At the surface, O_3 values at Hyderabad showed a clear decrease from May to August, which was not observed in Guangzhou and Nanjing. In this section, we investigate ground station data during the monsoon of 2011 over five different locations (see Fig. 3, in red). We distinguish between the Indian and Chinese stations by the sampling method. The three Indian stations shown here are provided with monthly means only. The two Chinese sites are a collection of stations and have hourly values: the data from the Pearl River Delta is the daily average of 12 stations, and the data from the North China Plain site are daily average over 7 stations. Details on the location, type and sampling method of the Indian and Chinese stations as well as discussion of each of the Chinese station data are provided in the Supplement. Figure 6 shows the surface O_3 VMR for the Indian ground stations in panel a and for the Chinese ground stations in panel b.

Both Hyderabad and Jabalpur show continuous decreasing O_3 values from May till August, of total magnitude of 22 and 20 ppbv respectively. Hyderabad decreasing O_3

ACPD
15, 31925–31950, 2015

values are in agreement with the MOZAIC data at the surface as seen in Fig. 5 (the MOZAIC O_3 profile is taken at Rajiv Gandhi International Airport, located around 25 km away from the ground surface station). On the other hand, Udaipur shows a smaller monsoon signature and O_3 values decrease of 5 ppbv between May and July and then increase back in August to 32 ppbv. The Indian stations geographic locations explain the observed monthly variation. If we look at the location of the stations and at Fig. 2, we can see how Hyderabad and Jabalpur are affected by the Indian summer monsoon, with strong winds and high cloud cover explaining the decrease detected. Udaipur lies in a region where the monsoon is milder, leading to a small decrease in the summertime O_3 values. The values detected over these three stations are also reflected in the IASI [0–6] km O_3 column, which exhibits the largest decrease in India, except in the north-west region, the area where Udaipur is located. Panel b station data are the 24-h running average (and the associated standard deviation in shaded blue) of 12 stations in the PRD region and 7 stations in the NCP region. Since we are interested in the regional EASM effect on O_3, we show the average of the stations here (the station are between 25 to 300 km away). For details and more timely resolved observations for each of the station, please see the Supplement.

The ground observations of the PRD stations in panel b detect a decrease of around 25 ppbv from May to June coinciding with when the northwesterly winds from the Pacific become stronger (see Fig. 2). The O_3 VMR increase slightly afterwards in July and August due to the decrease in monsoon strength over this region (also seen in Fig. 2). Panel b for the NCP stations show a weak monthly decrease in O_3 concentrations from June to July and August of 5–10 ppbv. The IASI and meteorological data presented in Fig. 2, also suggest the same decreasing pattern in O_3 concentrations driven by the slight increase in cloud cover.

ACPD
15, 31925–31950, 2015

4 Conclusions

The East Asian Summer Monsoon plays an important role in changing the pollutants concentration as well as the weather and climate system over the monsoon regions leading to effects on the global air quality and climate system (Rodwell and Hoskins, 2001). The study of the dynamics and variability of the East Asian monsoon provides useful information to analyze the distribution and losses of pollutants such as tropospheric O_3. The latter is shown to have a particular seasonal variation over south and East Asia due to the monsoon. This study shows that the monsoon variability is recorded and well captured over the different years by the infrared remote sensor IASI during [2008–2013]. The IASI [0–6] km O_3 columns decrease starting the months of May/June of each year, and reach a minimum in July–August. This decrease is most prominent in south Asia where the monsoon is stronger. In order to assess the monsoon meteorological signature on tropospheric O_3, we compare tropospheric O_3 to cloud cover, relative humidity and wind fields from the ERA-interim archive during the monsoon of 2011 taken as an example year. Clear inverse relationship is seen between the IASI [0–6] km tropospheric O_3 on one hand and cloud cover and winds on the other hand. This explained by the fact that the high cloud cover that the monsoon generates, accompanied with high relative humidity in the troposphere lead to a lower production rate since the photochemical activity will be much lower and relative humidity is a sink of O_3 in particular in the background troposphere. On the other hand, the winds are also strong during the monsoon and O_3 during this period can be transported either vertically due to deep convection to above the [0–6] km column, or horizontally to/from the Pacific and to the globe. Validation of the IASI-O_3 columns with aircraft data shows a good correlation (r = 0.74) between the [0–6] km columns from IASI to that derived from aircraft profiles. A monsoon signature is detected on the O_3 profile, in particular in the lower troposphere, in Hyderabad, Guangzhou and Nanjing that are in agreement with the IASI [0–6] km O_3 column spatial distribution. Ground station measurements of O_3 also show spatial dependence and are anti-correlated to the EASM strength. The

ACPD
15, 31925–31950, 2015

stations in central and north India as well as in Pearl River Delta show a signature of the monsoon on ground O_3 that can be explained by the change in meteorology over these regions. In northwest India, and the North China plain, winds are weaker, and the cloud cover is smaller and thus the ground O_3 shows a smaller decrease during the EASM.

More generally, this study shows that in lack of good coverage of ground and aircraft measurements, satellite observations, such as the one provided in this work using IASI, provide valuable information that could help investigating the regional and global monsoon impact on the distribution of pollutants in the troposphere and in particular tropospheric O_3. With IASI-C to be launched in 2018 onboard MetOp-C and a new series of three IASI-NG instruments on MetOp Second Generation Satellites around 2022 (Crevoisier et al., 2014), long term IASI O_3 time series obtained at high spatial resolution will be available to characterize and detect the onset and the progression of the monsoon.

The Supplement related to this article is available online at doi:10.5194/acpd-15-31925-2015-supplement.

Acknowledgements. IASI is a joint mission of EUMETSAT and the Centre National d'Etudes Spatiales (CNES, France). The IASI L1 data are distributed in near real time by EUMETSAT through the EumetCast system distribution. MOZAIC is presently funded by INSU-CNRS (France), Météo-France, Université Paul Sabatier (Toulouse, France) and Research Center Jülich (FZJ, Jülich, Germany). IAGOS has been and is additionally funded by the EU projects IAGOS-DS and IAGOS-ERI. The authors acknowledge the strong support of the European Commission, Airbus, and the Airlines (Lufthansa, Air-France, Austrian, Air Namibia, Cathay Pacific, Iberia and China Airlines so far) who carry the MOZAIC or IAGOS equipment and perform the maintenance since 1994. The authors are grateful to the ETHER database (http://www.pole-ether.fr) for providing the IASI L1C data and L2 temperature data. This study was carried out in the framework of the "East Asian Monsoon and air quality" project, which is a part of the DRAGON program (http://dragon3.esa.int), the EU-FP7 PANDA project

ACPD
15, 31925–31950, 2015

(http://www.marcopolo-panda.eu/), the EUMETSAT O3M-SAF project, and the ESA O_3 Climate Change Initiative (O_3-CCI). The French scientists are grateful to CNES and Centre National de la Recherche Scientifique (CNRS) for financial support. The research in Belgium is funded by the Belgian State Federal Office for Scientific, Technical and Cultural Affairs and the European Space Agency (ESA Prodex arrangement). P. F. Coheur is Senior Research Associate with F.R.S-FNRS.

References

Akimoto, H.: Global air quality and pollution, Science, 302, 1717–1719, 2003.

Barret, B., Le Flochmoen, E., Sauvage, B., Pavelin, E., Matricardi, M., and Cammas, J. P.: The detection of post-monsoon tropospheric ozone variability over south Asia using IASI data, Atmos. Chem. Phys., 11, 9533–9548, doi:10.5194/acp-11-9533-2011, 2011.

Chan, L. Y., Liu, H. Y., Lam, K. S., Wang, T., Oltmans, S. J., and Harris, J. M.: Analysis of the seasonal behavior of tropospheric ozone at Hong Kong, Atmos. Environ., 32, 159–168, doi:10.1016/S1352-2310(97)00320-8, 1998.

Clarisse, L., R'Honi, Y., Coheur, P. F., Hurtmans, D., and Clerbaux, C.: Thermal infrared nadir observations of 24 atmospheric gases, Geophys. Res. Lett., 38, 1–5, doi:10.1029/2011GL047271, 2011.

Clerbaux, C., Boynard, A., Clarisse, L., George, M., Hadji-Lazaro, J., Herbin, H., Hurtmans, D., Pommier, M., Razavi, A., Turquety, S., Wespes, C., and Coheur, P.-F.: Monitoring of atmospheric composition using the thermal infrared IASI/MetOp sounder, Atmos. Chem. Phys., 9, 6041–6054, doi:10.5194/acp-9-6041-2009, 2009.

Coheur, P.-F., Clarisse, L., Turquety, S., Hurtmans, D., and Clerbaux, C.: IASI measurements of reactive trace species in biomass burning plumes, Atmos. Chem. Phys., 9, 5655–5667, doi:10.5194/acp-9-5655-2009, 2009.

Cooper, O. R., Parrish, D. D., Ziemke, J., Balashov, N. V., Cupeiro, M., Galbally, I. E., Gilge, S., Horowitz, L., Jensen, N. R., Lamarque, J.-F., Naik, V., Oltmans, S. J., Schwab, J., Shindell, D. T., Thompson, a. M., Thouret, V., Wang, Y. and Zbinden, R. M.: Global distribution and trends of tropospheric ozone: An observation-based review, Elem. Sci. Anthr., 2, 000029, doi:10.12952/journal.elementa.000029, 2014.

ACPD
15, 31925–31950, 2015

Crevoisier, C., Clerbaux, C., Guidard, V., Phulpin, T., Armante, R., Barret, B., Camy-Peyret, C., Chaboureau, J.-P., Coheur, P.-F., Crépeau, L., Dufour, G., Labonnote, L., Lavanant, L., Hadji-Lazaro, J., Herbin, H., Jacquinet-Husson, N., Payan, S., Péquignot, E., Pierangelo, C., Sellitto, P., and Stubenrauch, C.: Towards IASI-New Generation (IASI-NG): impact of improved spectral resolution and radiometric noise on the retrieval of thermodynamic, chemistry and climate variables, Atmos. Meas. Tech., 7, 4367–4385, doi:10.5194/amt-7-4367-2014, 2014.

Dee, D. P., Uppala, S. M., Simmons, A. J., Berrisford, P., Poli, P., Kobayashi, S., Andrae, U., Balmaseda, M. A., Balsamo, G., Bauer, P., Bechtold, P., Beljaars, A. C. M., van de Berg, L., Bidlot, J., Bormann, N., Delsol, C., Dragani, R., Fuentes, M., Geer, A. J., Haimberger, L., Healy, S. B., Hersbach, H., Holm, E. V, Isaksen, L., Kallberg, P., Kohler, M., Matricardi, M., McNally, A. P., Monge-Sanz, B. M., Morcrette, J.-J., Park, B.-K., Peubey, C., de Rosnay, P., Tavolato, C., Thepaut, J.-N., and Vitart, F.: The ERA-Interim reanalysis: configuration and performance of the data assimilation system, Q. J. Roy. Meteor. Soc., 137, 553–597, doi:10.1002/qj.828, 2011.

Ding, A. J., Wang, T., Thouret, V., Cammas, J.-P., and Nédélec, P.: Tropospheric ozone climatology over Beijing: analysis of aircraft data from the MOZAIC program, Atmos. Chem. Phys., 8, 1–13, doi:10.5194/acp-8-1-2008, 2008.

Ding, A. J., Fu, C. B., Yang, X. Q., Sun, J. N., Zheng, L. F., Xie, Y. N., Herrmann, E., Nie, W., Petäjä, T., Kerminen, V.-M., and Kulmala, M.: Ozone and fine particle in the western Yangtze River Delta: an overview of 1 yr data at the SORPES station, Atmos. Chem. Phys., 13, 5813–5830, doi:10.5194/acp-13-5813-2013, 2013.

Dufour, G., Eremenko, M., Orphal, J., and Flaud, J.-M.: IASI observations of seasonal and day-to-day variations of tropospheric ozone over three highly populated areas of China: Beijing, Shanghai, and Hong Kong, Atmos. Chem. Phys., 10, 3787–3801, doi:10.5194/acp-10-3787-2010, 2010.

Dufour, G., Eremenko, M., Griesfeller, A., Barret, B., LeFlochmoën, E., Clerbaux, C., Hadji-Lazaro, J., Coheur, P.-F., and Hurtmans, D.: Validation of three different scientific ozone products retrieved from IASI spectra using ozonesondes, Atmos. Meas. Tech., 5, 611–630, doi:10.5194/amt-5-611-2012, 2012.

Dufour, G., Eremenko, M., Cuesta, J., Doche, C., Foret, G., Beekmann, M., Cheiney, A., Wang, Y., Cai, Z., Liu, Y., Takigawa, M., Kanaya, Y., and Flaud, J.-M.: Springtime daily variations in lower-tropospheric ozone over east Asia: the role of cyclonic activity and pollution as

ACPD
15, 31925–31950, 2015

observed from space with IASI, Atmos. Chem. Phys., 15, 10839–10856, doi:10.5194/acp-15-10839-2015, 2015.
Hurtmans, D., Coheur, P. F., Wespes, C., Clarisse, L., Scharf, O., Clerbaux, C., Hadji-Lazaro, J., George, M., and Turquety, S.: FORLI radiative transfer and retrieval code for IASI, J. Quant. Spectrosc. Ra., 113, 1391–1408, doi:10.1016/j.jqsrt.2012.02.036, 2012.
Johnson, C. E., Collins, W. J., Stevenson, D. S., and Derwent, R. G.: Relative roles of climate and emissions changes on future tropospheric oxidant concentrations, J. Geophys. Res.-Atmos., 104, 18631–18645, doi:10.1029/1999JD900204, 1999.
Lal, D. M., Sachin, D. G., Patil, S. D., Kulkarni, S. H., Jena, C., Tiwari, S., and Srivastava, M. K.: Tropospheric ozone and aerosol long-term trends over the Indo-Gangetic Plain (IGP), India, Atmos. Res., 116, 82–92, doi:10.1016/j.atmosres.2012.02.014, 2012.
Lam, K. S., Wang, T. J., Chan, L. Y., Wang, T., and Harris, J.: Flow patterns influencing the seasonal behavior of surface ozone and carbon monoxide at a coastal site near Hong Kong, Atmos. Environ., 35, 3121–3135, doi:10.1016/S1352-2310(00)00559-8, 2001.
Lawrence, M. G. and Lelieveld, J.: Atmospheric pollutant outflow from southern Asia: a review, Atmos. Chem. Phys., 10, 11017–11096, doi:10.5194/acp-10-11017-2010, 2010.
Marenco, A., Thouret, V., Nédélec, P., Smit, H., Helten, M., Kley, D., Karcher, F., Simon, P., Law, K., Pyle, J., Poschmann, G., Von Wrede, R., Hume, C., and Cook, T.: Measurement of ozone and water vapor by Airbus in-service aircraft: The MOZAIC airborne program, an overview, J. Geophys. Res., 103, 25631, doi:10.1029/98JD00977, 1998.
McPeters, R. D., Labow, G. J., and Logan, J. A.: Ozone climatological profiles for satellite retrieval algorithms, J. Geophys. Res.-Atmos., 112, D05308, doi:10.1029/2005JD006823, 2007.
Nedelec, P., Blot, R., Boulanger, D., Athier, G., Cousin, J.-M., Gautron, B., Petzold, A., Volz-Thomas, A., and Thouret, V.: Instrumentation on commercial aircraft for monitoring the atmospheric composition on a global scale?: the IAGOS system, technical overview of ozone and carbon monoxide measurements, Tellus B, 67, 27791, doi:10.3402/tellusb.v67.27791, 2015.
Ohara, T., Akimoto, H., Kurokawa, J., Horii, N., Yamaji, K., Yan, X., and Hayasaka, T.: An Asian emission inventory of anthropogenic emission sources for the period 1980–2020, Atmos. Chem. Phys., 7, 4419–4444, doi:10.5194/acp-7-4419-2007, 2007.
Parthasarathy, B., Munot, A. A., and Kothawale, D. R.: All-India monthly and seasonal rainfall series: 1871–1993, Theor. Appl. Climatol., 49, 217–224, doi:10.1007/BF00867461, 1994.

ACPD
15, 31925–31950, 2015

Richter, A., Burrows, J. P., Nu, H., Granier, C., and Niemeier, U.: Increase in tropospheric nitrogen dioxide over China observed from space, Lett. Nat., 437, 129–132, doi:10.1038/nature04092, 2005.

Richter, A., Hilboll, A., and Burrows, J. P.: Revisiting satellite derived tropospheric NO_2 trends, Poster presentation submitted to the EGU meeting, Geophys. Res. Abstr., EGU2015-10674, EGU General Assembly 2015, Vienna, Austria, 2015.

Rodgers, C.: Inverse Methods for Atmospheric Sounding: Theory and Practice, Series on Atmospheric, Oceanic and Planetary Physics, Vol. 2, World Scientific, Hackensack, 2000.

Rodwell, M. J. and Hoskins, B. J.: Subtropical anticyclones and summer monsoons, J. Climate, 14, 3192–3211, 2001.

Safieddine, S., Clerbaux, C., George, M., Hadji-Lazaro, J., Hurtmans, D., Coheur, P. F., Wespes, C., Loyola, D., Valks, P., and Hao, N.: Tropospheric ozone and nitrogen dioxide measurements in urban and rural regions as seen by IASI and GOME-2, J. Geophys. Res.-Atmos., 118, 10555–10566, doi:10.1002/jgrd.50669, 2013.

Safieddine, S., Boynard, A., Coheur, P.-F., Hurtmans, D., Pfister, G., Quennehen, B., Thomas, J. L., Raut, J.-C., Law, K. S., Klimont, Z., Hadji-Lazaro, J., George, M., and Clerbaux, C.: Summertime tropospheric ozone assessment over the Mediterranean region using the thermal infrared IASI/MetOp sounder and the WRF-Chem model, Atmos. Chem. Phys., 14, 10119–10131, doi:10.5194/acp-14-10119-2014, 2014.

Thouret, V., Marenco, A., Sabatier, P., Logan, J. A., Ndec, P., Grouhel, C. and Sabatier, P.: Comparisons of ozone measurements from the MOZAIC airborne program and the ozone sounding network at eight locations, J. Geophys. Res., 103, 25695–25720, doi:10.1029/98JD02243, 1998.

Van der A., R. J., Eskes, H. J., Boersma, K. F., van Noije, T. P. C., Van Roozendael, M., De Smedt, I., Peters, D. H. M. U., and Meijer, E. W.: Trends, seasonal variability and dominant NO_x source derived from a ten year record of NO_2 measured from space, J. Geophys. Res.-Atmos., 113, 1–12, doi:10.1029/2007JD009021, 2008.

Wang, B. and Fan, Z.: Choice of South Asian summer monsoon indices, B. Am. Meteorol. Soc., 80, 629–638, 1999.

Wang, B., Ding, Q., and Joseph, P. V: Objective definition of the Indian summer monsoon onset, J. Climate, 22, 3303–3316, doi:10.1175/2008JCLI2675.1, 2009.

ACPD
15, 31925–31950, 2015

Wang, T., Wei, X. L., Ding, A. J., Poon, C. N., Lam, K. S., Li, Y. S., Chan, L. Y., and Anson, M.: Increasing surface ozone concentrations in the background atmosphere of Southern China, 1994–2007, Atmos. Chem. Phys., 9, 6217–6227, doi:10.5194/acp-9-6217-2009, 2009.
Wang, Y., McElroy, M. B., Munger, J. W., Hao, J., Ma, H., Nielsen, C. P. and Chen, Y.: Variations of O_3 and CO in summertime at a rural site near Beijing, Atmos. Chem. Phys., 8(21), 6355–6363, doi:10.5194/acp-8-6355-2008, 2008.
Worden, J., Jones, D. B. A., Liu, J., Parrington, M., Bowman, K., Stajner, I., Beer, R., Jiang, J., Thouret, V., Kulawik, S., Li, J.-L. F., Verma, S., and Worden, H.: Observed vertical distribution of tropospheric ozone during the Asian summertime monsoon, J. Geophys. Res.-Atmos., 114, D13304, doi:10.1029/2008JD010560, 2009.
Xu, X., Lin, W., Wang, T., Yan, P., Tang, J., Meng, Z., and Wang, Y.: Long-term trend of surface ozone at a regional background station in eastern China 1991–2006: enhanced variability, Atmos. Chem. Phys., 8, 2595–2607, doi:10.5194/acp-8-2595-2008, 2008.
Yang, S. and Lau, K.-M.: Influences of Sea Surface Temperature and Ground Wetness on Asian Summer Monsoon, J. Climate, 11, 3230–3246, 1998.
Yang, Y., Liao, H., and Li, J.: Impacts of the East Asian summer monsoon on interannual variations of summertime surface-layer ozone concentrations over China, Atmos. Chem. Phys., 14, 6867–6879, doi:10.5194/acp-14-6867-2014, 2014.
Zhao, C., Wang, Y., Yang, Q., Fu, R., Cunnold, D., and Choi, Y.: Impact of East Asian summer monsoon on the air quality over China: View from space, J. Geophys. Res.-Atmos., 115, 1–12, doi:10.1029/2009JD012745, 2010.
Zhou, D., Ding, A., Mao, H., Fu, C., Wang, T., Chan, L. Y., Ding, K., Zhang, Y., Liu, J., Lu, A., and Hao, N.: Impacts of the East Asian monsoon on lower tropospheric ozone over coastal South China, Environ. Res. Lett., 8, 44011, doi:10.1088/1748-9326/8/4/044011, 2013.

ACPD
15, 31925–31950, 2015

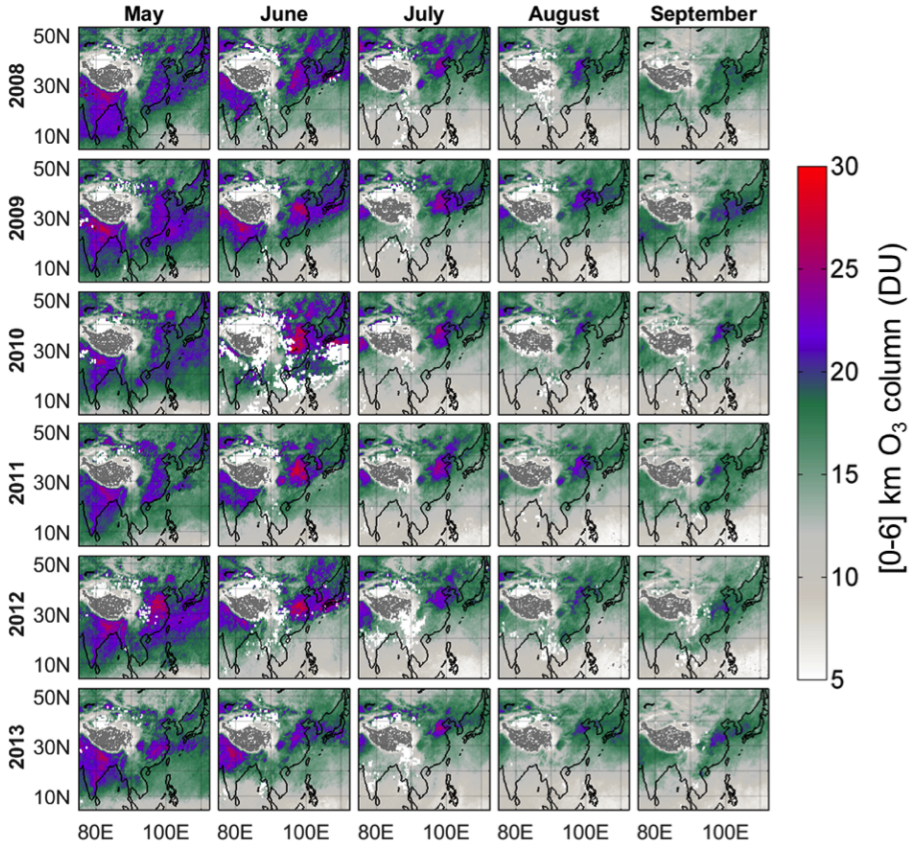

Figure 1. Monthly averaged daytime tropospheric [0–6] km O_3 column from IASI over the EASM region and period (May–September) for the years 2008–2013. The decrease due to the monsoon is more prominent to the south of the domain.

ACPD
15, 31925–31950, 2015

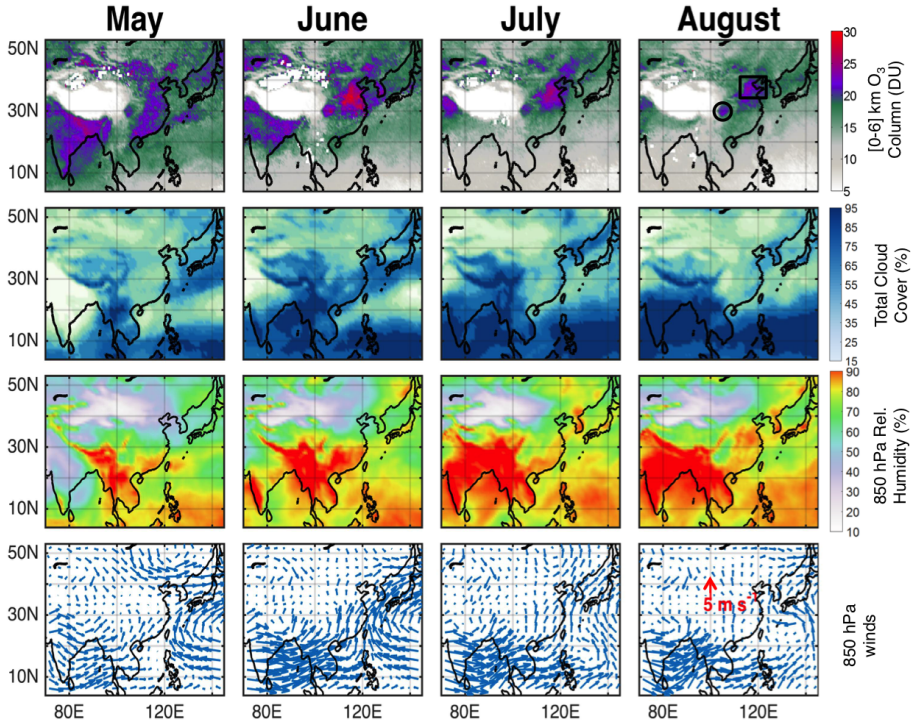

Figure 2. Monthly averaged tropospheric [0–6] km O_3 column from IASI, along with ECMWF total cloud cover, relative humidity and winds at 850 hPa for each of the months of May to August 2011. The black square and circle (upper right plot) are the regions the least affected by the EASM and discussed more in the text.

ACPD
15, 31925–31950, 2015

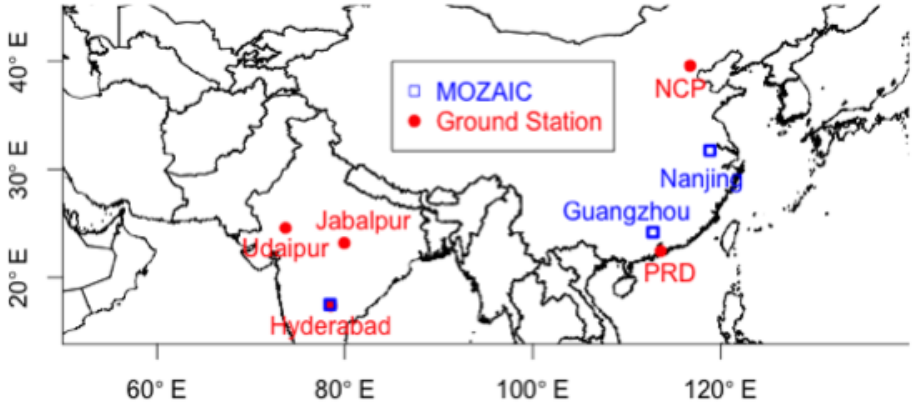

Figure 3. Location of the MOZAIC flight data at the airports of Hyderabad, Guangzhou and Nanjing used in this section and represented with blue squares. In red are represented the location of the ground stations used in Sect. 3.3. Note that at Hyderabad, we have both ground station and aircraft data (around 25 km away from one another).

ACPD
15, 31925–31950, 2015

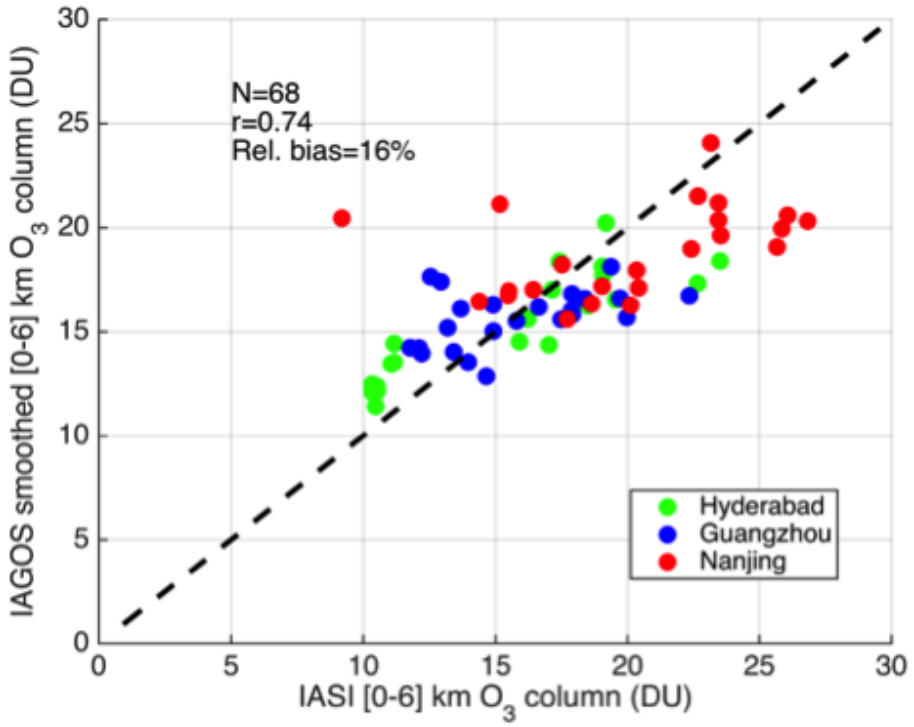

Figure 4. The [0–6] km O_3 columns retrieved from IASI correlation with 68 coincident MOZAIC profiles convolved with IASI averaging kernels for the period May–August 2011 over Hyderabad, Guangzhou and Nanjing.

ACPD
15, 31925–31950, 2015

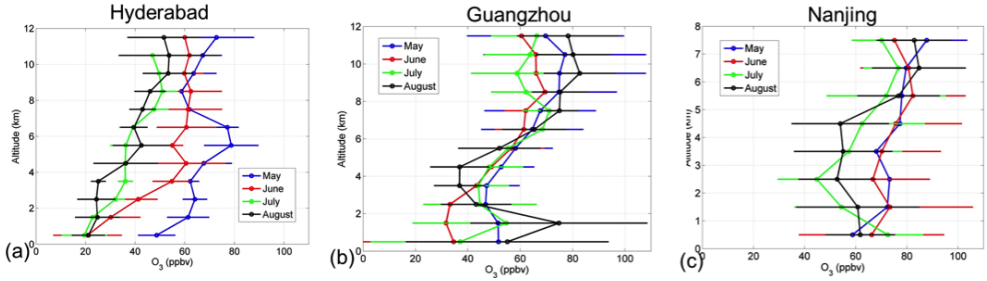

Figure 5. Monthly averaged vertical profiles of tropospheric O_3 from MOZAIC during the period May–August 2011 at **(a)** Hyderabad, **(b)** Guangzhou and **(c)** Nanjing. Error bars correspond to the standard deviation.

ACPD
15, 31925–31950, 2015

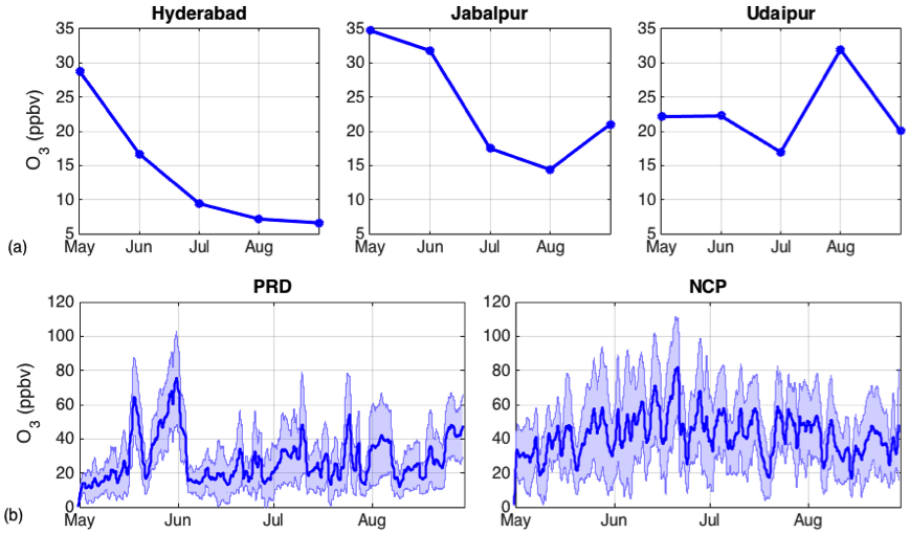

Figure 6. Ground station data during the EASM of 2011 over India: Hyderabad, Udaipur and Jabalpur in **(a)**; and over China, Pearl River Delta (PRD), and North China Plain (NCP) in **(b)**. The shaded region in **(b)** corresponds to the standard deviation of the 24-h running average of the different stations in the PRD and NCP sites respectively. The location of the stations is plotted in Fig. 3, and more information is provided in the Supplement.

ACPD
15, 31925–31950, 2015